Environ. Sci. Technol. **1998**, *32,* 2009−2017

Experiments and Modeling of the Transport of Trichloroethene Vapor in Unsaturated Aquifer Material

SEAN W. LORDEN,[†,§] WENLIN CHEN,[‡] AND LEONARD W. LION*,[†]

School of Civil and Environmental Engineering, Cornell University, Ithaca, New York 14853, and Novartis Crop Protection, Inc., Environmental Safety Department, P.O. Box 18300, Greensboro, North Carolina 27419-8300

A bench-scale reactor system was used to investigate mass-transfer dynamics and transport of trichloroethene (TCE) vapor in a column of unsaturated aquifer material under conditions of advective gas flow, at 25 °C and 90% relative humidity. Two gas flows (40 and 80 mL/min) and two relative vapor pressures of TCE (10% and 90% P/P_0, where P is vapor pressure and P_0 is the saturation vapor pressure) were selected as experimental variables. Breakthrough curves were generated for week-long inputs of TCE-laden air and for short pulses of a nonsorbing tracer gas. Equilibrium sorption isotherms for TCE were also measured and used as tools for interpreting the column experiment results. Slow mass-transfer kinetics were observed in all of the transport experiments. Evidence from the breakthrough curves and the sorption isotherms suggested that, at 90% P/P_0, a significant amount of TCE was condensed in pores or sorbed at the gas−water interface. Desorption and volatilization of interfacially sorbed TCE appeared to be rapid processes. The applicability of a recently developed mathematical transport model using a statistical γ distribution of desorption rate constants was tested using the experimental data. The γ distribution provides two adjustable parameters to account for sorption site heterogeneity and multiple mechanisms of sorption. When fit to the breakthrough curve obtained at high flow and high relative pressure, the model successfully predicted TCE frontal breakthrough and elution profiles at all other experimental conditions with no adjustable parameters. The predictive capability of the γ model was shown to be superior to that of two commonly used alternative model paradigms: the two-site first-order and two-site spherical diffusion models.

Introduction

One of the most persistent environmental problems that municipalities, industries, and government agencies currently face is remediation of contaminated soil, and the most frequently detected soil pollutants are classified as volatile organic compounds (VOCs) (*1*−*4*). VOCs partition into the soil, water, and gas compartments of the subsurface environment, and given time, the VOC phase distribution tends toward an equilibrium condition. Important factors that control the equilibrium phase distribution include the compound's aqueous solubility, Henry's law constant, and saturated vapor pressure. Soil properties, such as the sorptive affinity for the compound and the soil moisture and gas content, will also influence the phase distribution. In addition, interactions between the components of mixtures of different VOCs can be important. The effects of these and other factors have been studied by many investigators and are described in the literature (e.g., refs *5*−*11*).

When advective gas flow is induced in the subsurface environment, as it is in the remediation process known as soil vapor extraction, there will be a net rate of transfer of VOC molecules from the stationary phase to the mobile phase, or vice versa, depending on the initial conditions. A major challenge confronted in planning remediation systems is the prediction of their duration, which depends on the rate of VOC transfer to the gas phase. This difficulty arises, in part, because multiple mechanisms govern mass transfer between the stationary moist porous media and mobile gas phase, and because the porous medium is typically heterogeneous with respect to its physical structure as well as its sorptive properties. In unsaturated soil, possible mass-transfer processes for VOCs include hindered diffusion in microporous soil particles and soil organic matter, diffusion in pore water and soil-bound water films, and mass transfer at the gas−water interface. This array of transport mechanisms is expected to proceed deterministically inward (during sorption) or outward (during desorption) in series on a given microscopic section of the porous medium. The overall serial transfer rate (*12*), however, may vary drastically in a random manner from point to point due to the complexity in soil microgeometry and the distribution of organic matter, pore water, and other sorptive components.

Several mathematical models have been proposed to describe heterogeneous mass-transfer processes under water-saturated soil conditions. These include the two-site first-order (TSFO) model (*13*), the two-site spherical diffusion (TSSD, or particle diffusion) model (*14*, *15*), and the γ-distributed site model (GS) (*16*−*19*). A common approach in these models is that the serial multiple mass transfer mechanisms are lumped into a single-rate process at a given microscopic sorptive surface. They differ, however, in the macroscopic descriptions of sorption heterogeneity across the population of all possible microscopic surfaces. Both TSFO and TSSD models assume two distinct sorption domains: one associated with instantaneous sorption and the other accounting for a time-dependent process. The time-dependent process is simplified as a first-order process in the TSFO model, while it is assumed to be diffusion in a uniform sorbing sphere in the TSSD model. A more general approach is adopted by the GS model in which the population of all possible microscopic surfaces is described by a probability distribution: the γ distribution function. The γ distribution is a convenient and flexible unimodel function that has met with prior success in the description of contaminant desorption from soil (*16*, *19*). The positively valued γ distribution often arises as the distribution of "waiting time" for a total of n events to occur. The waiting time is analogous to the characteristic sorption time that defines the time required for a unit sorbed concentration change under a unit difference from equilibrium (*17*).

The objective of this study was to extend the above three sorption models to describe water-unsaturated conditions

* Corresponding author e-mail: LWL3@cornell.edu; phone: (607) 255-7571; fax: (607) 255-9004.

† Cornell University.

‡ Novartis Crop Protection, Inc.

§ Present address: Fluor Daniel GTI, Kennedy Business Park II, 431(F) Hayden Station Road, Windsor, CT, 06095.

S0013-936X(97)00921-8 CCC: $15.00
Published on Web 05/19/1998

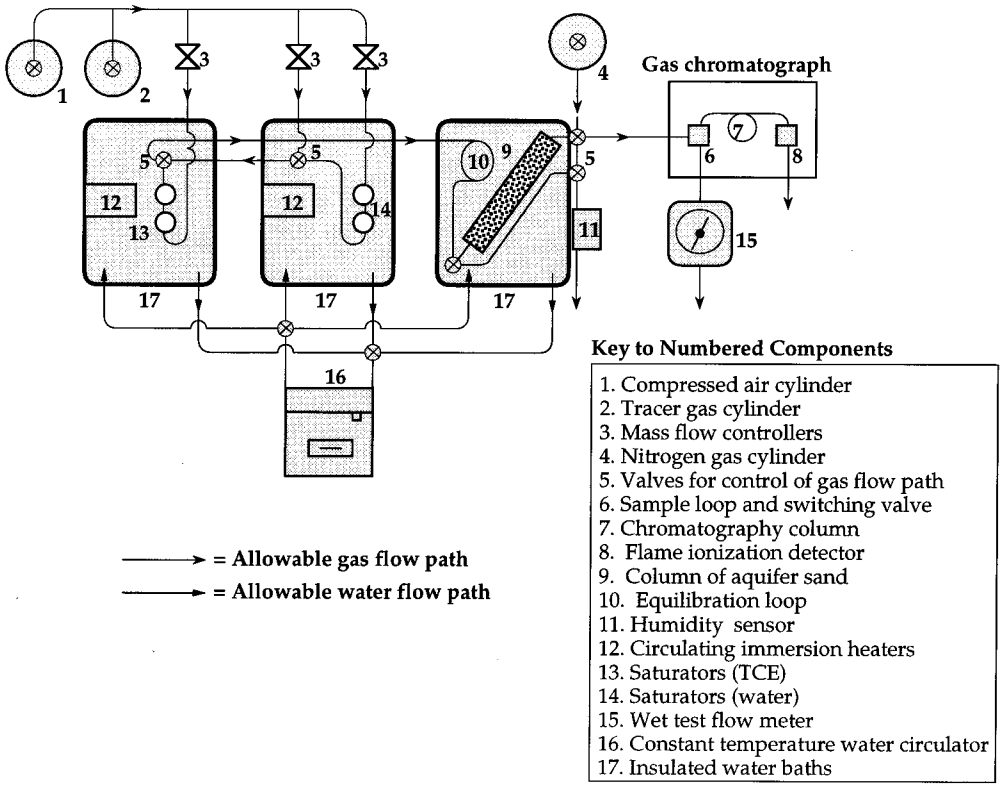

FIGURE 1. Experimental reactor.

where TCE vapor was induced to flow through a column packed with aquifer sand. TCE samples were collected over time at the exit of the column under two different flow rates and at two relative vapor pressures. The three sorption models, incorporated into the advective-dispersive equation (ADE), were applied to describe the measured TCE breakthrough curves (BTCs). Emphasis was placed on the overall BTC fit by a model and particularly on the relative abilities of the three models to predict the slow tailing of a BTC resulting from the influence of heterogeneous mass-transfer processes on the TCE nonequilibrium transport behavior.

Experimental Methods

Transport Experiments. *Sorbent.* A fine-grained aquifer sand obtained from a quarry in Newfield, NY, was used as the sorbent in this investigation. This sand has previously been characterized with respect to its N_2—BET specific surface area (3.3 m^2/g), organic carbon content (0.91%), and particle size distribution (93% sand, 6.3% silt) (see Chen et al. (*20*) for additional physical—chemical characteristics). Prior to conducting advective transport experiments, the sand was removed from a bulk storage container and allowed to air-dry from a field moisture content (MC) of approximately 4% to about 2 wt %. MC was checked by oven-drying samples of sand to a constant weight in a vacuum oven at 105 °C and −15 bar. A stainless steel column (38 cm long, 2.36 cm i.d.) was incrementally filled with the air-dried sand while the sides of the column were vibrated. After it was filled, the column was connected to the experimental apparatus (described below) and allowed to equilibrate to constant weight with a flowing gas stream at 90% relative humidity. Gravimetric measurements of the column of sand indicated a bulk density, a gas-filled porosity, and a MC of 1.29 g/cm^3, 0.52, and 1.6%, respectively. The gravimetric MC agreed closely with a value of 1.7% obtained by interpolation from a water desorption isotherm measured for the sand in preliminary experiments conducted as part of this investigation (*21*).

Experimental Reactor. A bench-scale reactor (Figure 1) was used to generate breakthrough curves for week-long periods. The reactor was adapted from an apparatus previously used for measuring equilibrium sorption of VOCs (*8*). Components of the reactor that were in contact with TCE were made of stainless steel, copper, brass, or glass. The only exceptions were valve seals of Teflon. All exposed tubing was insulated from ambient temperatures with foam or fiberglass insulation. Effluent gas from the column was directed into a Hewlett-Packard 5890 Series II gas chromatograph (GC) equipped with a flame ionization detector, and the gas was periodically sampled by means of an automated switching valve connected to a 0.25 cm^3 sample loop. One of the switching valve's outlet ports was connected to a wet test meter to verify the total flow rate delivered by the mass flow controllers. Sampling frequency was controlled by the GC's programmable timetable. The tubing and fittings between the column outlet and the switching valve were constrained to have a volume of no more than 10% of the total air-filled pore volume in the column of aquifer sand, thus minimizing dispersion not associated with flow through the sand itself.

Breakthrough Curves. Four sets of TCE breakthrough and elution profiles were generated (Table 1). The designations LC, LF, HC, and HF in Table 1 stand for low concentration, low flow, high concentration, and high flow, respectively. "High" and "low" are relative terms. The flow rates of 40 and 80 mL/min were chosen so that the resulting pore velocity of the gas would fall within the range of 0.001 m/s to 0.008 m/s. This range is thought to be representative of the range of velocities attained during soil vapor extraction at remediation sites (*22*). The TCE vapor concentrations of 90% P/P_o (472.5 mg/L) and 10% P/P_o (52.5 mg/L) correspond to the relative pressures that might be encountered in the "near field" close to a nonaqueous phase liquid (NAPL) source, and in the down-gradient "far field", respectively.

Two frontal breakthrough profiles were also generated for a nonsorbing tracer consisting of 4 vol % methane in

TABLE 1. Experimental Conditions and Soil TCE Concentrations (mg of TCE/g of Aquifer Material)

Experiment	LC-LF	LC-HF	HC-LF	HC-HF
TCE concentration (%P/P_o)	10	10	90	90
gas flux (mL/min)	40	80	40	80
total sorbed[a]	0.01	0.01	0.87	0.48
"partitioned"[b]	0.03	0.03	0.29	0.29
interfacially sorbed[c]	n/a	n/a	0.58	0.19
equilibrium capacity[d]	0.25	0.25	7.25	7.25

[a] Calculated from the area under the elution curve minus the amount present in the gas pore space at the beginning of the elution. [b] Calculated from K_d'. (Includes TCE dissolution into pore water and sorption from the pore water onto the aquifer material.) [c] Assumed equal to the difference between row 3 and row 4. [d] Calculated by interpolation from the TCE adsorption isotherm (see Figure 2).

nitrogen. Methane has been used as a nonsorbing tracer in similar types of experiments by other researchers (*23*, *24*).

The column of aquifer sand was maintained at 90% RH and 25 °C for all transport experiments. Breakthrough curves for TCE were generated from step function inputs. First, air laden with TCE was directed through the initially clean column of sand. This resulted in the frontal portion of the breakthrough curve, or the breakthrough profile. After frontal breakthrough was complete ($C/C_o = 1$ within the GC precision of ±2%), the column of sand was equilibrated with the flowing gas stream for a period of one week. During this period, effluent TCE concentrations, RH, and total flow rate were checked periodically to verify stable conditions. At the end of the equilibration period, the column of sand was isolated from the flowing gas stream with a bypass line (see Figure 1) in order to purge TCE from the reactor plumbing for a period of up to 2 h. Next, TCE-free air at 90% RH and 25 °C was used to purge the contaminated sand and facilitate desorption of TCE. This resulted in the back portion of the breakthrough curves, or the elution profiles. For tracer experiments, only the breakthrough profiles were generated. Between each transport experiment, the column of sand was purged with clean air at 90% RH for several days.

Equilibrium Sorption Experiments. A modified version of the quartz spring gravimetric adsorption apparatus described by Ong and Lion (*7*) was used to measure the adsorption of TCE on the sand at 90% RH and 25 °C across a wide range of TCE relative vapor pressures. The bulk sample distribution coefficients (K_D) for TCE at 10% and 90% P/P_o were obtained by linear interpolation between the adjacent measurements from the isotherm. The bulk distribution coefficients were subsequently compared with the total TCE sorption calculated from the area under the elution profile of the breakthrough curve (minus the amount of TCE present in the column pore space at the beginning of the elution profile).

Since the isotherm described above measured adsorption over a wide range of TCE relative pressures, processes such as adsorption and condensation at the gas−water interface might contribute to the measured adsorption of TCE (see additional discussion below). To assess the significance of these contributions, the expected distribution coefficient in the absence of condensation is calculated on the basis of the following analysis. At low values of P/P_o, it is reasonable to expect that the equilibrium distribution of TCE between the gas phase and that dissolved in the pore water is governed by a Henry's Law constant, and the aqueous solid phase sorption equilibrium of dissolved TCE also often obeys a linear distribution coefficient (*8*). Therefore, in the absence of vapor condensation and adsorption at the gas−water interface, the "partitioning" between the mobile gas and stationary (moist sand) phases is anticipated to be linear. The linear distribution coefficient (K_d') for TCE on the sand at the experimental moisture content of 1.6% was determined by measuring the saturated soil−water distribution coefficient (K_w = 0.20 mL/g (*21*)) using an established headspace technique (*8*, *25*) and applying the following relationship:

$$K_d' = \frac{K_w}{K_H} + \frac{(MC)}{100K_H} \quad (1)$$

where K_H is the dimensionless Henry's Law constant for TCE (K_H = 0.397 at 25 °C (*26*)) and MC is the moisture content of the aquifer sand (weight percent).

Equation 1 is reported to be valid in cases where the average surface coverage of water exceeds eight molecular layers (*7*). At the column moisture content of 1.6%, the aquifer sand used in this experiment was covered by approximately 18 molecular layers of water (based on the measured BET surface area of 3.3 m^2/g and a surface area of 10.8×10^{-20} m^2 for a water molecule (*27*)). Equation 1 was also experimentally verified by measuring K_d' for the aquifer material at a moisture content of 4.0%. The measured value of $K_d' = 0.60$ mL/g agreed directly with that calculated from eq 1 (*21*). The value of K_d' calculated from eq 1 for a moisture content of 1.6%, along with the total TCE sorption calculated from elution profiles, was used to estimate the amounts of "partitioned" TCE (TCE dissolved in pore water plus TCE sorbed from water to the sand) and TCE sorbed at the gas−water interface in the column experiments. It must be noted that the value of K_d' estimated by eq 1 is different from the bulk sample partitioning coefficient (K_D) determined from the experimental isotherm where TCE vapor condensation and other processes may have occurred at the gas−water interface.

Mathematical Modeling

The TSFO, TSSD, and GS sorption models and their incorporation into the ADE have been described in detail by Chen and Wagenet (*19*). The model development is briefly summarized here. The ADE under steady-state gas flow conditions is

$$\frac{\partial C}{\partial t} + \frac{\rho}{\theta}\frac{\partial S}{\partial t} + v\frac{\partial C}{\partial x} - D\frac{\partial^2 C}{\partial x^2} = 0 \quad (2)$$

where C is the TCE concentration (μg/mL), ρ is the column bulk density (g/cm^3), θ is the unfilled porosity (cm^3/cm^3), S is the sorbed concentration (μg/g), v is the gas pore velocity (cm/h), D is the dispersion coefficient (cm^2/h), t is the time (h), and x is the distance (cm).

Given the initial and boundary conditions,

$$C(x,t=0) = 0 \qquad S(x,t=0) = 0 \quad (3)$$

$$C(x=0,t) = C_o \qquad 0 < t < T_o;\ C(x=0,t) = 0,\ t > T_o \quad (4)$$

$$\text{and } C(x=\infty,t) = 0 \qquad t > 0 \quad (5)$$

where T_o is the input pulse length (h), Chen and Wagenet (*19*) have developed the Laplace domain solutions of eq 2 incorporated with the three sorption models described below.

The TSFO Model. This model assumes a linear isotherm for equilibrium sorption and a first-order mass-transfer process for the time-dependent sorption:

$$\frac{dS}{dt} = fK_D\frac{dC}{dt} + \frac{1}{T_s}[(1-f)K_DC - S_2] \quad (6)$$

where f is the fraction of equilibrium sorption sites, dimensionless; K_D is the bulk sample equilibrium distribution coefficient, mL/g; T_s is the characteristic time for sorption,

h, defined as the inverse of the first-order rate constant; and S_2 is the sorbed concentration in the time-dependent site, μg/g.

The TSSD Model. This model conceptualizes the time-dependent sorption in the TSFO model as a diffusion process in an idealized sorbing sphere representing the soil organic matrixes (intraorganic) (*15, 28*) or the microporous sorbent particles (intraparticle) (*14, 29*):

$$S = fK_D C + S_2 \tag{7}$$

$$S_2 = (1 - f)\frac{1 - \theta}{\rho}\frac{3}{a^3}\int_0^a r^2 S_o(x,r,t)\, dr \tag{8}$$

and

$$\frac{\partial S_o}{\partial t} = \frac{1}{T_d}\left(\frac{a}{r}\right)^2 \frac{\partial}{\partial r}\left(r^2 \frac{\partial S_o}{\partial r}\right) \tag{9}$$

where a is the radius of the spherical particle, cm; $S_o(x,r,t)$ represents the local TCE concentration in the sphere at a given position x and time t; r is the radius coordinate (cm); T_d is the characteristic time for diffusion (h), defined as a^2/D_e; and D_e is the effective diffusion coefficient (cm^2/h).

The GS Model. The GS model generalizes the two-site sorption heterogeneity to a continuum of sorption sites that are grouped into different classes according to a γ probability density function (pdf) for both equilibrium and rate parameters (*17, 18*). First-order sorption at a local site is described by

$$\frac{\partial S'}{\partial t} = \frac{1}{t_s}(K_d C - S') \tag{10}$$

where S' is the sorbed concentration of TCE at a local site (μg/g), t_s is the characteristic time for local sorption (h), and K_d is the local equilibrium distribution coefficient (mL/g). The statistical macroscopic average of all sorption sites is

$$S = \int_0^\infty \int S'(x,t) p_{ks}(K_d;t_s)\, dK_d\, dt_s \tag{11}$$

where p_{ks} is the joint pdf for K_d and t_s.

Assuming independent K_d and t_s, eq 11 becomes

$$S = K_D \int_0^\infty S'(x,t) p_s(t_s)\, dt_s \tag{12}$$

where p_s is the γ-pdf for t_s

$$p_s(t_s) = \frac{1}{\Gamma(n)}\beta^n t_s^{n-1} \exp(-\beta T_s) \tag{13}$$

and K_D here represents the average of all local K_d values of a bulk soil sample:

$$K_D = \int_0^\infty K_d p_k(K_d)\, dK_d \tag{14}$$

where p_k is a pdf of K_d. Note that in the γ-pdf, the parameters β and n determine the scale and shape of the distribution, respectively. Variations in these parameters render the distribution flexible and able to describe a range of skewed data. The mean and variance of the distribution are equal to n/β and n/β^2, respectively.

Subsequent modeling procedures involve curve-fitting and independent predictions. As a necessary condition for independent predictions, a model must be able to fit the experimental data. While a good curve fit is necessary, it is not sufficient. The conceptual basis of the model is tested when the model is required to simulate a set of experimental data using parameter values that are obtained independently.

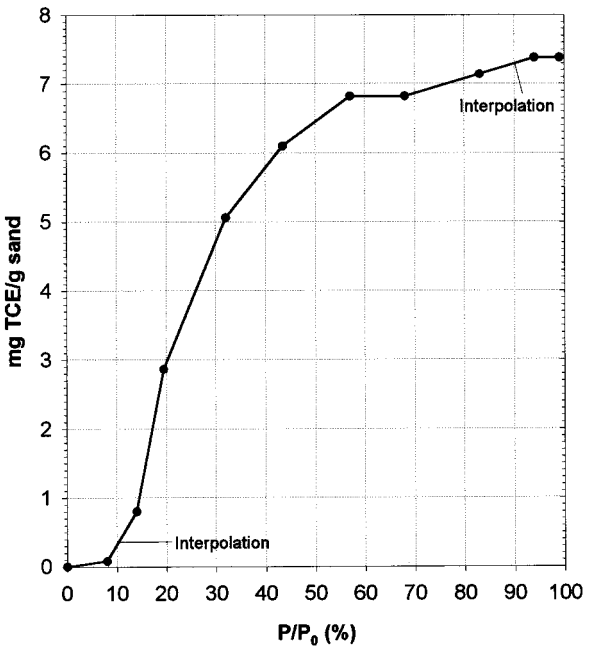

FIGURE 2. TCE adsorption on moist aquifer material at 90% RH and 25 °C.

In the present work, each model was used to fit all experimental data as a first test. Model ability to make independent predictions was then evaluated using a set of sorption parameters determined from a fit to an arbitrarily selected BTC (i.e., LC, HF) to predict other independent BTC data.

In the curve-fit process, a nonlinear least-squares (NLLS) technique was employed (*30*). The technique involved an iterative process in which model parameter values were adjusted automatically until the criterion of minimum deviation between model simulations and experimental data was achieved (*17*). To separate the advective transport process from sorption, transport-related parameters, v and D (or the Peclet number, $P = vL/D$, where L is column length), were determined independently using the BTC of the nonsorbing methane tracer. With P and v determined for each gas flux condition, the four TCE BTCs were used to determine the two sorption parameters of each model, that is, f and T_s for TSFO; f and T_d for TSSD; and n and β for GS. For each TCE curve fit, the BTC data were log-transformed to ensure sufficient weights for low concentrations in the BTC tailing profiles during the NLLS optimization process.

The macroscopic linear distribution coefficient K_D was independently obtained from the equilibrium sorption experiments. The K_D values corresponding to 10% and 90% relative TCE vapor pressures (at 25 °C and RH = 90%) were 4.8 and 15.3 mL/g, respectively, as obtained by linear interpolation between the adjacent measurement points. The K_D value could also have been estimated directly from the measured TCE BTCs, for example by the first moment analysis. However, such estimates are not independent of the column studies intended for modeling. In addition, the estimation is often subject to the sensitivity of BTC asymmetry, which is particularly true in severe nonequilibrium conditions where significantly high advective flow exists compared to relatively slow desorption. The K_D values calculated from moment analysis were consistently well below the isotherm values, suggesting that equilibrium was not attained in the column experiments.

Results and Discussion

The TCE adsorption isotherm (Figure 2) exhibited the characteristics of a type V isotherm as described by Gregg

and Sing (*31*). This type of isotherm is consistent with the sorption of a nonpolar sorbate on a polar, porous sorbent.

The total amounts of sorbed TCE as estimated from the areas under the column experiment elution profiles were all well below the equilibrium sorption capacities determined from the adsorption isotherm (Table 1). In a preliminary experiment a purged column was isolated for 5 days and the TCE concentration in the vapor phase was allowed to rebound and then purged again; however, the mass of TCE recovered increased by only 1%. This result suggests that the low values of total sorbed TCE were not artifacts of incomplete recovery during the elution phases of the BTCs. Despite the fact that total sorption remained well below the equilibrium sorptive capacity in the transport experiments, the BTCs were successfully modeled using linear distribution coefficients derived from the sorptive affinities obtained by interpolation of the adsorption isotherm (see below). Since the column was always far from equilibrium and under relatively strong advective-dispersive conditions, the treatment of the nonlinear sorption isotherm (Figure 2) as though it were linear did not have a significant impact on the ability of the model to predict the observed results. That is, the concentration dependency of the partitioning coefficient is not likely to have significant effects on the overall transport process under the severe nonequilibrium conditions.

Another interesting feature of the transport data is that the total sorbed TCE in the low-concentration experiments (LC-LF and LC-HF) remained below the equilibrium amount of "partitioned" TCE predicted by K_d' ($K_d' = 0.54$ at the column moisture content of 1.6%). If accumulation of TCE at the gas−water interface were to occur only after dissolution in pore water and sorption to the sand from the aqueous phase, this result would suggest that bound TCE was not significantly associated with the gas−water interface in the low-concentration transport experiments.

The total sorbed TCE significantly exceeded the amount of "partitioned" TCE predicted by K_d' in the high-concentration experiments (HC-LF and HC-HF), suggesting the presence of condensed-phase TCE (that could presumably exist because of the lower equilibrium vapor pressure of a curved TCE meniscus in small-diameter pores (*31*)) or TCE at the gas−water interface in these experiments. Since desorption of material from the interface would be expected to occur first, the early portion of the elution profile for the HC experiments should be governed by the kinetics for TCE vaporization and mass transfer at the gas−water interface. Interestingly, in both HC experiments the same duration (4.7 pore volumes) was required to recover the amounts of TCE estimated to be sorbed at the interface (0.58 and 0.19 μg/g, respectively). Therefore, given the long overall duration of the period needed for TCE elution, it seems reasonable to speculate that evaporation and desorption of TCE from the gas−water interface were relatively rapid kinetic processes.

In the low-concentration experiments, doubling the gas velocity did not seem to have a significant effect on the rate of mass transfer. The elution profiles for experiments LC-LF and LC-HF appear almost identical. The similarity of profiles for the low-concentration experiments at two different gas flows implies that mass transfer at the gas−water interface was not rate-limiting for sorption or desorption of TCE, and that a similar mechanism (such as diffusion in the aqueous phase) may have controlled mass-transfer kinetics at each gas flow velocity.

Doubling the gas velocity in the high-concentration experiments resulted in a more rapid approach to $C/C_o = 1$ during adsorption. The cumulative difference in terms of total mass sorbed becomes considerable as the number of elapsed pore volumes increases. It is likely that the relative importance of nonequilibrium sorption was increased at the higher gas flow velocity. Brusseau and Rao (*27*) have shown that an increase in nonequilibrium can cause earlier contaminant breakthrough.

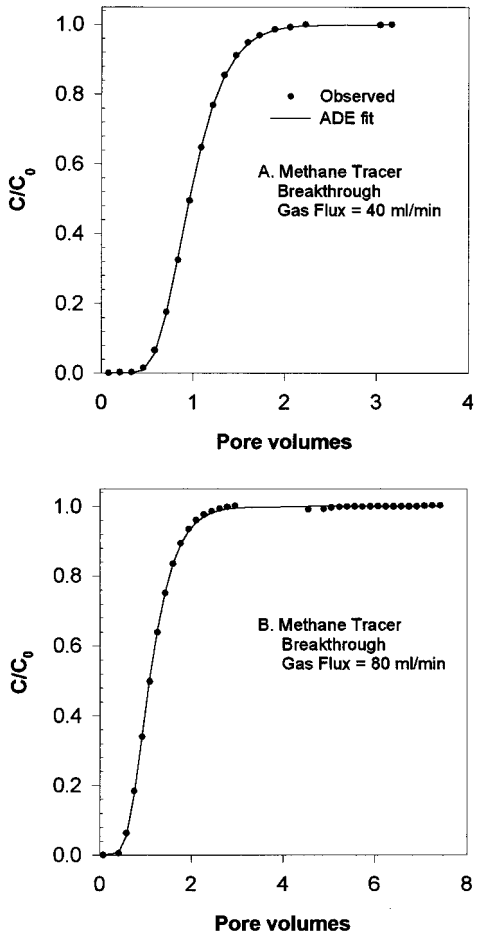

FIGURE 3. ADE fit to tracer BTCs. Parameters obtained were: v = 17.3 cm/min and P = 19.05 for a gas flux = 40 mL/min and v = 30.0 cm/min and P = 12.21 for a gas flux = 80 mL/min, respectively.

Modeling. The results of the curve fits of the two tracer BTCs are shown in Figure 3. The classical "S" shape of the BTCs and the good agreement between measurements and the ADE curve fits indicated that any nonequilibrium effects other than sorption such as the dead-end pore process either were insignificant or were well accounted for by the dispersion term. The two transport-related parameters, v and P, were 17.3 cm/min and 19.05 for the low gas flux experiment (40 mL/min), and 30.0 cm/min and 12.21 for the high gas flux experiment (80 mL/min), respectively.

Curve fitting of the four TCE experiments was performed by adjusting each model's two sorption parameters (Table 2). Fixed parameters during the curve-fitting process consisted of v and P, both determined from the tracer experiments at each corresponding flux condition, and the isotherm-interpolated K_D value at each TCE input relative pressure. As shown in Figure 4A−D, the agreement of the GS model with experimental data was superior to either the TSFO or the TSSD model in each of the four experimental cases. Note that the y axis is plotted on a log scale to emphasize model ability to fit the tails of the BTC. Of the three models, the TSFO was the least successful in describing the tailing behavior of the TCE desorption profiles.

The limitations of the TSFO and TSSD models were primarily reflected in the over predictions of concentrations in the tail of the desorption profiles. Both models, particularly the TSFO, failed to capture the gradual decline of the TCE concentrations. Over predictions of BTC tails suggested that a lower K_D value was likely required by the two models. Recall

TABLE 2. Results of Curve Fit by Each Sorption Model[a]

Model:	GS				TSFO				TSSD			
Exp.	β	n	K_D	SSD[b]	f	T_s	K_D	SSD[b]	f	T_d	K_D	SSD[b]
					2-parameter fit							
LC-LF	5.2×10^{-8}	0.40	fixed	133.9	0.95×10^{-7}	7522	fixed	145.2	9.2×10^{-11}	4203	fixed	484.7
LC−HF	5.3×10^{-13}	0.17	fixed	9.3	0.19	8264	fixed	31.4	2.7×10^{-6}	32190	fixed	220.9
HC-LF	1.8×10^{-8}	0.31	fixed	23.5	5.1×10^{-10}	6429	fixed	51.1	1.97×10^{-7}	28290	fixed	150.9
HC−HF	1.2×10^{-13}	0.17	fixed	7.4	2.9×10^{-3}	9000	fixed	37.6	2.9×10^{-3}	40050	fixed	202.7
					3-parameter fit							
LC-LF	nd[c]	nd	nd	nd	2.4×10^{-8}	299.8	0.140	143.5	2.3×10^{-9}	1023	0.139	140.7
LC-HF	nd	nd	nd	nd	0.088	29.8	0.070	15.6	1.0×10^{-5}	375.4	0.085	10.2
HC-LF	nd	nd	nd	nd	9.5×10^{-9}	165.5	0.624	38.0	5.2×10^{-10}	747.3	0.664	18.8
HC-HF	nd	nd	nd	nd	3.4×10^{-9}	50.5	0.165	11.6	4.5×10^{-7}	526.4	0.240	6.8

[a] Units: mL, min, and g. [b] SSD, the sum of squares of deviation between model and experimental data. [c] nd, not determined.

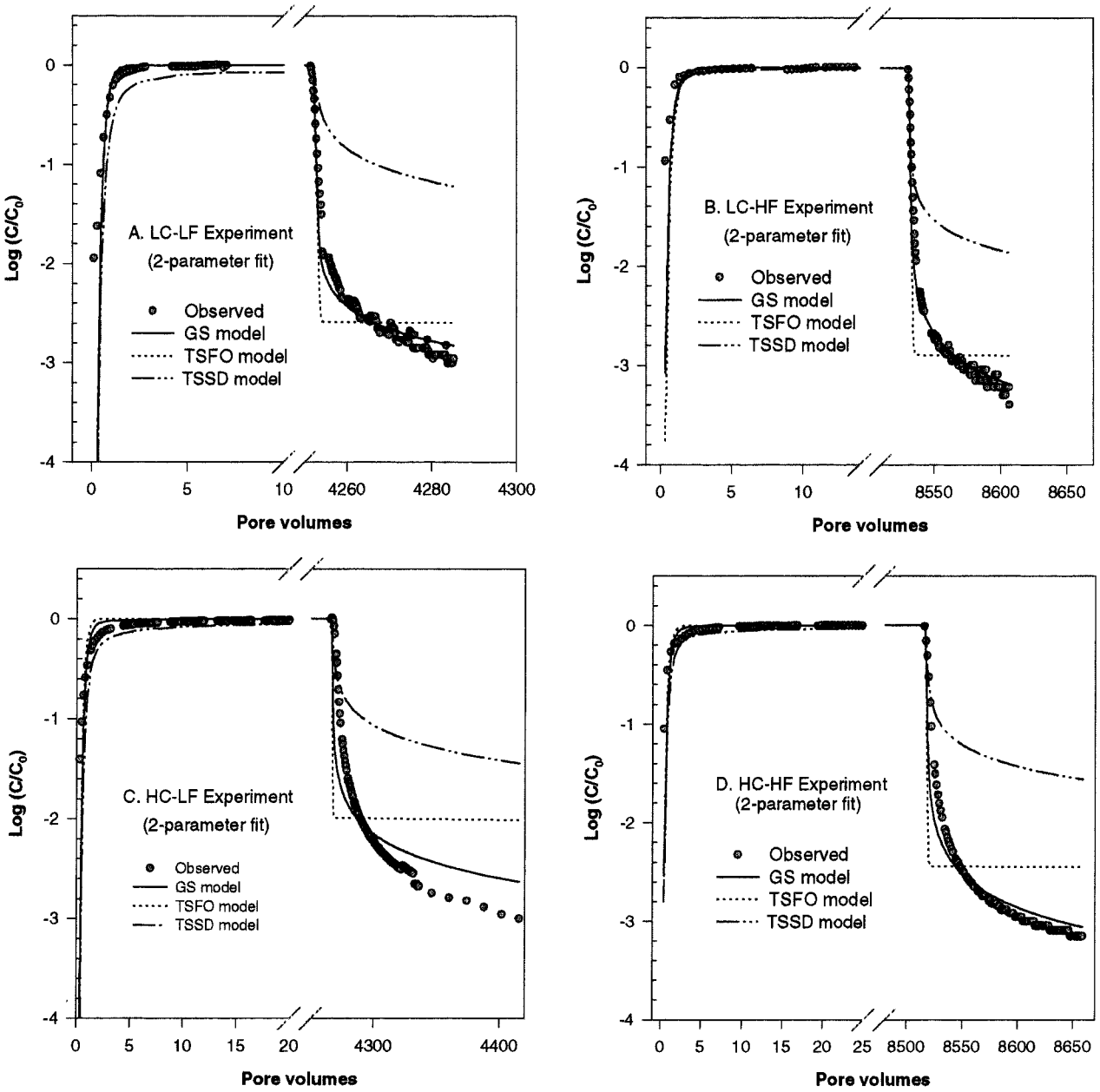

FIGURE 4. Model comparisons of 2-parameter fits. The K_D values were obtained from isotherm interpolation at the two different input relative pressures, that is, for $P/P_o = 10\%$, $K_D = 4.8$ mL/g (LC-LF and LC-HF); and for $P/P_o = 90\%$, $K_D = 15.3$ mL/g (HC-LF and HC-HF). Other fixed parameters (v and P) were obtained from the CH_4 tracer experiments (see Figure 3).

that the K_D values used were fixed to the numbers obtained from the batch isotherm, which were 4.8 and 15.3 mL/g for relative input pressures of 10% and 90%, respectively. As discussed previously, the isotherm-derived K_D values were

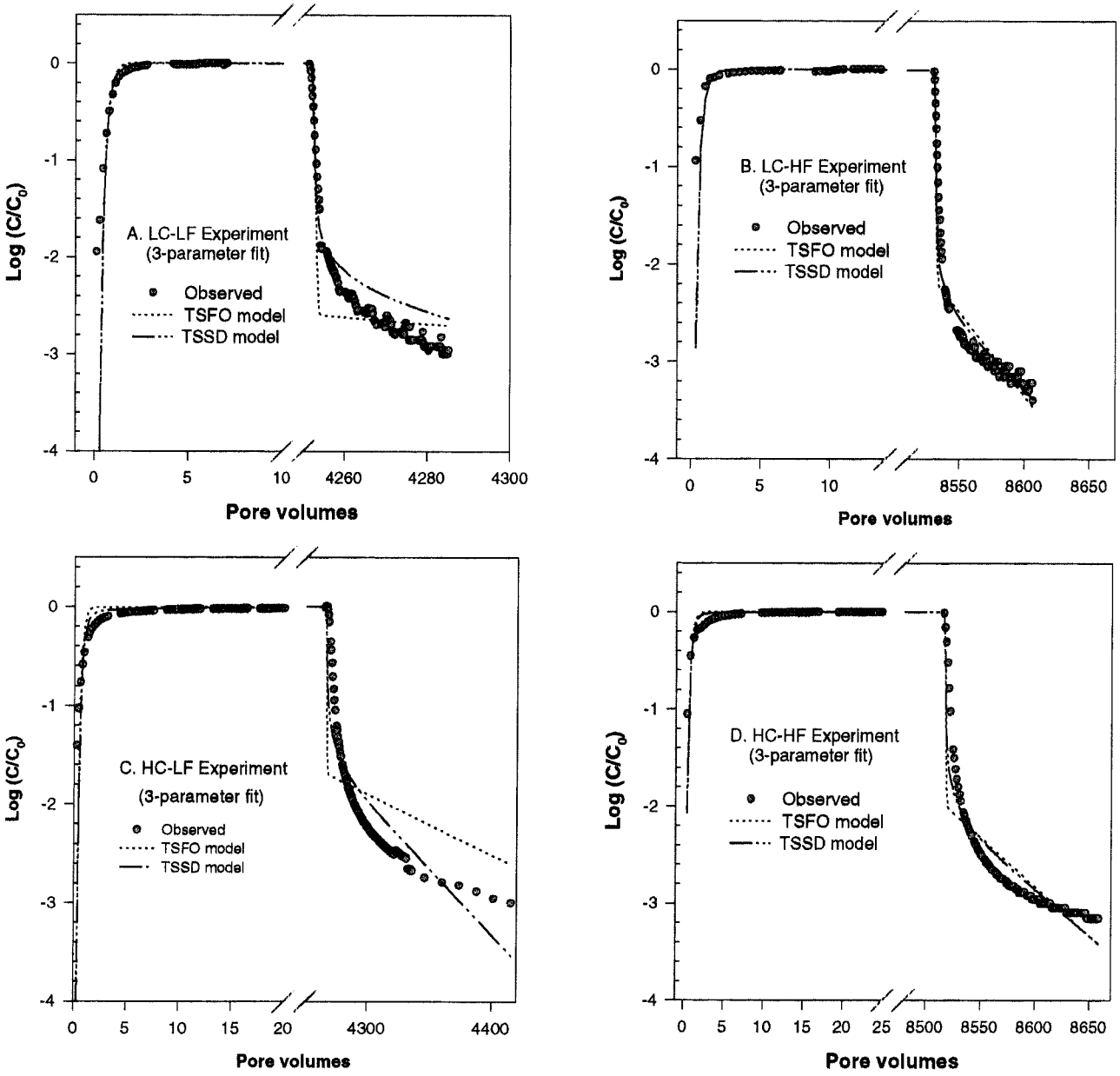

FIGURE 5. Model comparisons of 3-parameter fits by TSFO and TSSD. Other fixed parameters (*v* and *P*) were obtained from the CH_4 tracer experiments (see Figure 3).

substantially higher than the values derived from the first moment of the BTCs. To evaluate the possible effect of K_D on model performance, 3-parameter curve fits, including K_D as an additional adjustable parameter in TSFO and TSSD, were conducted for all TCE BTCs. The corresponding results are illustrated in Table 2 and Figure 5A−D.

While an obvious improvement in terms of the sum of squares of deviation (SSD) between model and measurements is seen from the 3-parameter fitting exercise for both TSFO and TSSD (Table 2), these two models still did not provide sufficiently accurate descriptions of the tail of the desorption curve (Figure 5A−D). Chen and Wagenet (*18*) have recently shown that two-site sorption models tend to provide sharp and straight concentration declines during advective transport when mass transfer is governed by slow desorption, which is simplified in the models as a single-rate process. This is particularly true when the single rate is assumed to be first-order such as in the TSFO model.

An interesting pattern in the fitted parameter values of K_D and T_s or T_d, by both TSFO and TSSD in the 3-parameter curve fits, is the velocity dependency of the parameter pair. As shown in Table 2, parameters T_s or T_d and K_D all tend to decrease as pore velocity increases for a same relative input pressure. For example, at the relative input pressure of 10% (i.e. the LC-LF and LC-HF experiments), the characteristic time for sorption T_s decreased from 299.8 to 29.8 min (or T_d from 1023 to 375.4 min) and the partition coefficient K_D was forced to change from 0.14 to 0.070 mL/g (or from 0.139 to 0.085 for the TSSD). A similar velocity dependency of the fitted parameters in two-site sorption models was observed in a water-saturated soil column study with atrazine by Chen and Wagenet (*19*) and was attributed to the lack of multiple sorption rates in the two models. It is intuitively obvious that if multiple sorption rate processes exist, it would be difficult to capture the behavior of time-dependent sorption under different advective flow conditions using a single-rate model. In such a dynamic system, the overall nonequilibrium condition can be represented by the ratio of the mean residence time of the advective flow to the characteristic sorption time (i.e., the Damkohler number). If a single

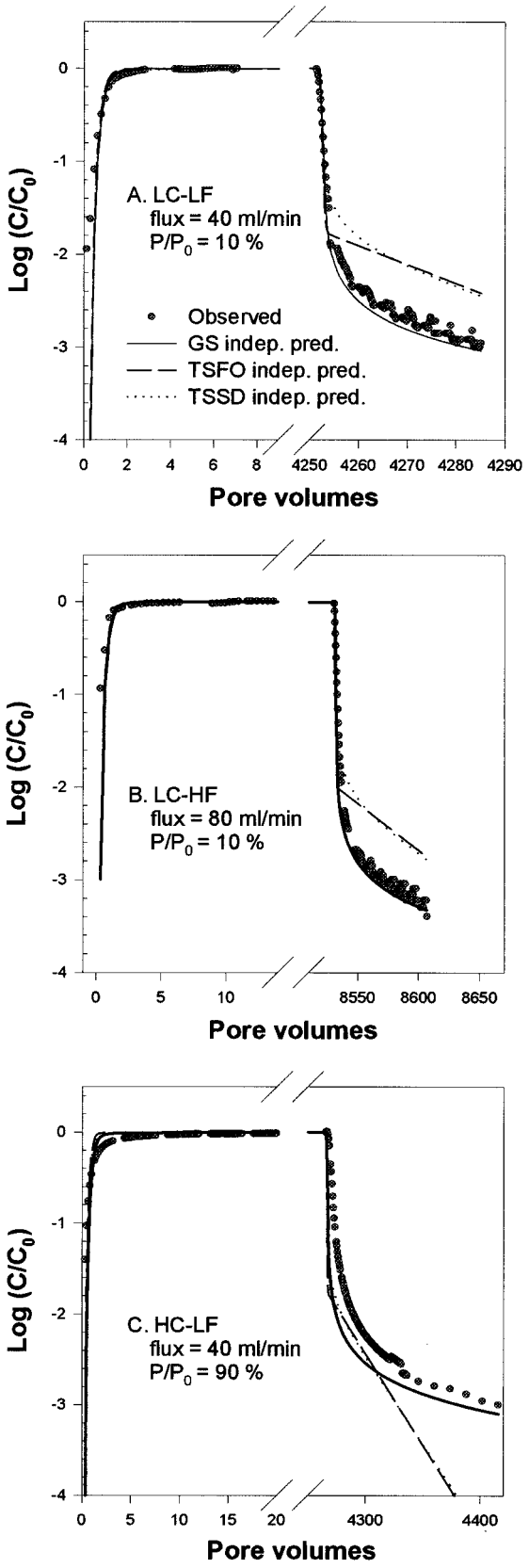

FIGURE 6. Model-independent predictions of the LC-LF, LC-HF, and HC-LF experiments using two fitted parameters (n and β) for the GS model and three fitted parameters for the TSFO and TSSD models (K_D, T_S, and f, and K_D, T_D, and f, respectively), all obtained from fits to the HC−HF experiment (see Table 2 for fitted values).

sorption rate exists (i.e., a constant characteristic sorption time), a less severe nonequilibrium condition and a larger Damkohler number would be expected to result as flow velocity decreases.

To further test model ability for independent predictions, the GS model was applied to make predictions of the LC-LF, LC-HF, and HC-LF experiments using the two sorption parameters (n and β) obtained from the BTC fit of the HC-HF experiment (Figure 6A−C) and the isotherm-interpolated K_D value corresponding to each relative input pressure. As shown in the figures, excellent agreements between model predictions and measurements were achieved, except that there was some underestimation of the desorption profile in the HC-LF experiment (Figure 6C).

Independent predictions by TSFO and TSSD of the LC-LF, LC-HF, and HC-LF experiments using the 3-parameter fitted values of the HC-HF are also shown in Figure 6A−C. The three fitted parameters were $K_D = 0.165$ mL/g, $T_s = 50.5$ min, and $f = 3.4 \times 10^{-9}$ for TSFO; and $K_D = 0.24$ mL/g, $T_d = 526.4$ min, and $f = 4.5 \times 10^{-7}$ for TSSD. As shown in the figures, none of the predictions were able to reconcile the gradually declining desorption tails. The sharp and straight declines predicted by both models underscore the velocity dependence of these two models and suggest that different kinetic controls may be operating under different advective flow conditions.

In summary, the GS sorption model outperformed the other two modeling approaches, TSFO and TSSD, given the same number of adjustable parameters for describing slow-sorption processes. The GS model also outperformed the other two models even when those models were allowed an additional adjustable parameter. A greater number of mechanistic governing processes is likely to be involved in the sorption of vapors versus those governing sorption under saturated conditions. Sorptive processes unique to vapors include condensation and sorption at the gas−water interface. The GS model as developed for water-saturated cases appears readily applicable to unsaturated conditions.

Acknowledgments

This research was supported by the Air Force Office of Scientific Research, USAF, under grant number F49620-94-1-0157.

Literature Cited

(1) Page, G. W. *Environ. Sci. Technol.* **1981**, *15*, 1475−1481.
(2) Westrick, J. J.; Mello, J. W.; Thomas, R. F. *J.—Am. Water Works Assoc.* **1984**, *76* (5), 52−59.
(3) Kerfoot, H. B., In *Soil Vapor Extraction Technology Reference Handbook*; U.S. EPA: Washington, DC, 1991; EPA/540/2-91/003.
(4) Conant, B. H.; Gilham, R. W.; Mendoza, C. A. *Water Resour. Res.* **1996**, *32*, 9−22.
(5) Amali, S.; Petersen, L. W.; Rolston, D. E. *J. Hazard. Mater.* **1994**, *36*, 89−108.
(6) Rhue, R. D.; Pennell, K. D.; Reve, W. H.; Hornsby, A. G. *J. Environ. Qual.* **1993**, *22*, 521−527.
(7) Ong, S. K.; Lion, L. W. *Soil Sci. Soc. Am. J.* **1991**, *55*, 1559−1568.
(8) Ong, S. K.; Lion, L. W. *J. Environ. Qual.* **1991**, *20*, 180−188.
(9) Ong, S. K.; Culver, T. B.; Lion, L. W.; Shoemaker, C. A. *J. Contam. Hydrol.* **1992**, *11*, 273−290.
(10) Thoms, S. R.; Lion, L. W. *Chemosphere* **1992**, *25*, 1707−1719.
(11) Valsaraj, K. T.; Thibodeaux, L. J. *J. Hazard. Mater.* **1988**, *19*, 79−99.
(12) Brusseau, M. L.; Jessup, R. E., Rao, P. S. C. *Water Resour. Res.* **1989**, *25*, 1971−1988.
(13) van Genuchten, M. T.; Wagenet, R. J. *Soil Sci. Soc. Am. J.* **1989**, *53*, 1303−1310.
(14) Ball, W. P.; Roberts, P. V. *Environ. Sci. Technol.* **1991**, *25*, 1237−1249.
(15) Pignatello, J. J.; Fernandino, F. J.; Huang, L. Q. *Environ. Sci. Technol.* **1993**, *27*, 1563−1571.
(16) Connaughton, D. F.; Stedinger, J.; Lion, L. W.; Shuler, M. L. *Environ. Sci. Technol.* **1993**, *27*, 2397−2403.
(17) Chen, W. Ph.D. Thesis, Cornell University, 1994.

(18) Chen, W.; Wagenet, R. J. *Environ. Sci. Technol.* **1995**, *29*, 2725−2734.
(19) Chen, W.; Wagenet, R. J. *Soil Sci. Soc. Am. J.* **1997**, *61*, 360−371.
(20) Chen, J.-H.; Lion, L. W.; Ghiorse, W. C.; Shuler, M. L. *Water Res.* **1995**, *29*, 421−430.
(21) Lorden, S. W. M.S. Thesis, Cornell University, School of Civil and Environmental Engineering, 1996.
(22) Grathwohl, P.; Reinhard, M. *Environ. Sci. Technol.* **1993**, *27*, 2360−2366.
(23) Farrell, R. E.; Germida, J. J.; Huang, P. M. *Appl. Environ. Microbiol.* **1993**, *59*, 1507−1514.
(24) Gierke, J. S.; Hutzler, N. J.; McKenzie, D. B. *Water Resour. Res.* **1992**, *28*, 323−335.
(25) Peterson, M. S.; Lion, L. W.; Shoemaker, C. A. *Environ. Sci. Technol.* **1988**, *22*, 571−578.
(26) Garbarini, D. R.; Lion, L. W. *Environ. Sci. Technol.* **1985**, *19*, 1122−1128.
(27) Livingston, H. F. *J. Colloid Sci.* **1949**, *4*, 447−458.
(28) Brusseau, M. L.; Rao, P. S. C. *Crit. Rev. Environ. Cont.* **1989**, *19*, 33−99.
(29) Wu, S. C.; Gschwend, P. M. *Environ. Sci. Technol.* **1986**, *20*, 717−725.
(30) Marquardt, D. L. *J. Soc. Ind. Appl. Math* **1963**, 2, 431−441.
(31) Gregg, S. J.; Sing, K. S. W. *Adsorption, Surface Area and Porosity*; Academic Press: New York, 1982.

Received for review October 20, 1997. Revised manuscript received April 7, 1998. Accepted April 13, 1998.

ES970921I